

Demonstration of the nearly continuous operation of an ^{171}Yb optical lattice clock for half a year

Takumi Kobayashi¹, Daisuke Akamatsu¹, Kazumoto Hosaka¹,
Yusuke Hisai², Masato Wada¹, Hajime Inaba¹, Tomonari
Suzuyama¹, Feng-Lei Hong², Masami Yasuda¹

¹National Metrology Institute of Japan (NMIJ), National Institute of Advanced
Industrial Science and Technology (AIST), 1-1-1 Umezono, Tsukuba, Ibaraki
305-8563, Japan

²Department of Physics, Graduate School of Engineering Science, Yokohama
National University, 79-5 Tokiwadai, Hodogaya-ku, Yokohama 240-8501, Japan

E-mail: takumi-kobayashi@aist.go.jp

Abstract. Optical lattice clocks surpass primary Cs microwave clocks in frequency stability and accuracy, and are promising candidates for a redefinition of the second in the International System of Units (SI). However, the robustness of optical lattice clocks has not yet reached a level comparable to that of Cs fountain clocks which contribute to International Atomic Time (TAI) by the nearly continuous operation. In this paper, we report the long-term operation of an ^{171}Yb optical lattice clock with a coverage of 80.3% for half a year including uptimes of 93.9% for the first 24 days and 92.6% for the last 35 days. This enables a nearly dead-time-free frequency comparison of the optical lattice clock with TAI over months, which provides a link to the SI second with an uncertainty of low 10^{-16} . By using this link, the absolute frequency of the $^1\text{S}_0-^3\text{P}_0$ clock transition of ^{171}Yb is measured as 518 295 836 590 863.54(26) Hz with a fractional uncertainty of 5.0×10^{-16} . This value is in agreement with the recommended frequency of ^{171}Yb as a secondary representation of the second.

1. Introduction

Several optical lattice clocks have achieved fractional frequency stabilities and uncertainties at the 10^{-18} level [1–5], which is better than primary Cs fountain microwave clocks. These achievements have stimulated discussion regarding a redefinition of the second in the International System of Units (SI) [6–9].

With the aim of redefining the SI second, the absolute frequencies of optical lattice clocks have been measured by many groups and used to determine the recommended frequencies of secondary representations of the second [8]. The absolute frequency can be directly measured referenced to a Cs fountain clock if it is locally available in the laboratory [10–15]. When a local Cs clock is not available, the absolute frequency

can be measured using a satellite link to International Atomic Time (TAI). TAI is a global timescale computed by the Bureau International des Poids et Mesures (BIPM). BIPM provides the frequency difference between TAI and the SI second averaged over a month. Therefore, the continuous comparison of an optical clock with TAI for a month is desirable in terms of linking to the SI second without additional uncertainty resulting from the dead time. A long-term comparison is also needed to reduce the uncertainty arising from the satellite link [16]. Since optical lattice clocks have commonly been operated intermittently, previous works have mostly employed stable local flywheels (e.g, an ensemble of hydrogen masers) that reach the 10^{-16} level to bridge the gaps in the operation of the lattice clocks [17–20]. A few groups have reported the nearly continuous operation of Sr optical lattice clocks with uptimes of 93% for 10 days, 83% for three weeks [14], and 84% for 25 days [21].

The continuous operation of an optical lattice clock is essential for the calibration of the frequency of TAI as a secondary representation of the second [8] as well as the absolute frequency measurement. A robust lattice clock is also important for new applications including tests of fundamental physics [12, 19, 22–26], relativistic geodesy [27, 28], and the generation of a stable local timescale [13, 29–31].

The main challenge as regards realizing the continuous operation of an optical lattice clock is to stabilize the frequencies of several light sources including an optical frequency comb to allow the comparison of the optical clock and a microwave standard. So far, we have developed multi-branch erbium-doped-fiber-based frequency combs that can run continuously for long periods [32]. By stabilizing the frequencies of many light sources to the comb, we have constructed a simple and reliable laser system for clock experiments [33]. We have also developed a relocking scheme [34] for optical phase locking. These techniques should greatly assist the realization of the continuous operation.

In this paper, we report the operation of an ^{171}Yb optical lattice clock with a coverage of 80.3% for half a year (185 days) including uptimes of 93.9% for the first 24 days, 86.4% for the second 27 days, 80.4% for the third 30 days, 72.7% for the fourth 35 days, 82.6% for the fifth 25 days, and 92.6% for the sixth 35 days. Using a single hydrogen maser with its stability limited by a flicker floor of 2×10^{-15} , we reduce the uncertainty in the link between the Yb clock and the SI second to the low 10^{-16} level, and measure the absolute frequency of the Yb clock transition.

2. Experimental setup

Figure 1 is a schematic diagram of the experimental setup. The setup for the Yb optical lattice clock is similar to that reported in our previous paper [35]. The clock utilizes the $^1\text{S}_0 - ^3\text{P}_0$ clock transition at 578 nm of ^{171}Yb atoms trapped in an optical lattice operated at the magic wavelength [36] of 759 nm. The 578 nm light was generated by the second harmonic generation (SHG) of an external cavity diode laser (ECDL) emitting at 1156 nm [37]. The lattice light at 759 nm was provided by a titanium sapphire (Ti:S) laser

(M squared, SolsTiS-4000-SRX-R). Before loading the atoms to the optical lattice, two-stage laser cooling with the $^1\text{S}_0$ – $^1\text{P}_1$ transition at 399 nm and the $^1\text{S}_0$ – $^3\text{P}_1$ transition at 556 nm was carried out to decrease the temperature of the atoms to several tens of microkelvins. The 399 nm light was generated by an injection-locked 399 nm diode laser with an automatic relocking mechanism [38]. A seed light for the injection locking was provided by the SHG of a 798 nm ECDL [39]. The 556 nm light for the second stage cooling was prepared by the SHG of a 1112 nm light from a fiber laser (NKT Photonics, Koheras) with a semiconductor optical amplifier. All the SHG processes were performed with single-pass periodically poled LiNbO₃ waveguides.

The 1112 nm fiber laser and the 1156 nm ECDL were phase locked to a narrow linewidth fiber comb (Fiber comb 1 in Fig. 1) [40,41]. This comb was phase locked to a master Nd:YAG laser at 1064 nm, which was stabilized to an ultra-low expansion (ULE) cavity by using the Pound-Drever-Hall method. To compensate for the narrow capture range of optical phase locking, a recently-developed relocking scheme [34] was incorporated in the phase locking of the comb to the master laser and the phase locking of the 1112 nm and 1156 nm lasers to the comb. The 798 nm ECDL and the Ti:S laser were stabilized to another fiber comb (Fiber comb 2 in Fig. 1) by frequency locking with an electrical delay line [42], which ensured a large capture range. Fiber comb 2 was referenced to the Coordinated Universal Time of the National Metrology Institute of

Japan (UTC(NMIJ)), which is generated by a hydrogen maser and an auxiliary output generator to add an arbitrary frequency offset.

The Yb optical lattice clock was operated with a cycle time of about 1.7 s. Yb atoms effused from an oven were decelerated with a Zeeman slower and cooled in first-stage cooling for about 1.2 s and then further cooled in second-stage cooling for 275 ms. In the present work, a window heated at 204°C was installed inside a vacuum chamber in the pass of the Zeeman slower beam to prevent the atomic beam from coating the viewport. The atoms were then loaded into a vertically oriented one-dimensional optical lattice and spin-polarized with the 1S_0 – 3P_1 transition at 556 nm for 20 ms. A Rabi π pulse resonant on the clock transition was then applied for 40 ms. The atomic population and the excitation probability were deduced using a laser-induced fluorescence signal by the 1S_0 – 1P_1 transition at 399 nm, and repumping on the 3P_0 – 3D_1 transition at 1389 nm induced by a free-running distributed feedback laser. The excitation probability was used to calculate frequency corrections applied for an acousto-optic modulator (AOM), which steers the frequency of the clock laser to the atomic transition. The atomic transition was split into two Zeeman components $m_F = \pm 1/2$ by applying a bias magnetic field of 65 μ T. The clock laser was stabilized to each component.

Fiber comb 2 was also used to measure the frequency of the Yb clock against UTC(NMIJ). To transfer the stability of UTC(NMIJ) to the comb without degradation, we mixed the 7th harmonics of the repetition rate frequency $f_{\text{rep}} \sim 121.8$ MHz with a 900 MHz signal which was generated by the 90-fold frequency multiplication of a 10 MHz signal from UTC(NMIJ). The resulting output frequency from the mixer $\delta \sim 47$ MHz was phase locked to a synthesizer referenced to UTC(NMIJ). After stabilizing the comb to UTC(NMIJ), the beat frequency between the clock laser and the comb was measured by using a zero dead-time frequency counter.

3. Demonstration of the nearly continuous operation

The frequency of the Yb optical lattice clock was measured against UTC(NMIJ) during a half-year period from the Modified Julian Date (MJD) 58754 (28 September 2019) to MJD 58939 (31 March 2020). The Yb clock was operated with uptimes of 93.9% in the first 24-day campaign from MJD 58754 to MJD 58778, 86.4% in the second 27-day campaign from MJD 58787 to MJD 58814, 80.4% in the third 30-day campaign from MJD 58814 to MJD 58844, 72.7% in the fourth 35-day campaign from MJD 58844 to MJD 58879, 82.6% in the fifth 25-day campaign from MJD 58879 to MJD 58904, and 92.6% in the sixth 35-day campaign from MJD 58904 to MJD 58939 (see also Table 1). Figures 2 (a) - (f) respectively show the fractional frequency differences between the Yb clock and UTC(NMIJ), denoted by $y(\text{Yb} - \text{UTC(NMIJ)})$, in the first - sixth campaigns. The uptime was calculated by using $N_{\text{valid}}T_{\text{cycle}}/T_{\text{total}}$, where N_{valid} is the number of valid data points, T_{cycle} the clock cycle time (~ 1.7 s), and T_{total} the total period of the measurement. We discarded data that included the following events: (i) large excursions in the phase-locked frequencies that can occur during the relocking

procedures; (ii) cycle slips in the frequency counting; and (iii) low excitation probabilities of the clock transition that lasted for a sufficiently long period.

The fractional frequency difference $y(\text{Yb} - \text{UTC}(\text{NMIJ}))$ is given by

$$\begin{aligned} y(\text{Yb} - \text{UTC}(\text{NMIJ})) &= \frac{f^a(\text{Yb})}{f^n(\text{Yb})} - \frac{f^a(\text{UTC}(\text{NMIJ}))}{f^n(\text{UTC}(\text{NMIJ}))} \\ &\approx \frac{f^a(\text{Yb})/f^a(\text{UTC}(\text{NMIJ}))}{f^n(\text{Yb})/f^n(\text{UTC}(\text{NMIJ}))} - 1, \end{aligned} \quad (1)$$

where $f^{a(n)}(X)$ denotes the actual (nominal) frequency of X . The approximation is valid when $(f^a(X) - f^n(X)) \ll f^n(X)$. Here we chose $f^n(\text{UTC}(\text{NMIJ})) = 10$ MHz and $f^n(\text{Yb}) = f^{\text{CIPM}}(\text{Yb}) = 518\,295\,836\,590\,863.6$ Hz, which is the CIPM (Comité International des Poids et Mesures) recommended frequency of ^{171}Yb [8].

Table 1. Uptimes of the Yb optical lattice clock

Campaign	MJD	Period (days)	Uptime (%)
1	58754 - 58778	24	93.9
2	58787 - 58814	27	86.4
3	58814 - 58844	30	80.4
4	58844 - 58879	35	72.7
5	58879 - 58904	25	82.6
6	58904 - 58939	35	92.6
Total	58754 - 58939	185	80.3

The clock was mostly unattended during the full campaign period. Several experimental parameters were monitored remotely. A data acquisition computer automatically sent an email alert to operators when one of the experimental parameters was outside the normal range. In the first campaign (see Fig. 2 (a)), to demonstrate almost dead-time-free operation ($\geq 90\%$ uptime per day), we always carried out manual tuning as soon as we received the email alert. Significant reductions in the uptime were caused by rare events such as the passage of a typhoon at MJD 58770 and the breaking of a diode laser used in fiber comb 1 at MJD 58778. In the second to sixth campaigns (see Figs. 2 (b)-(f)), manual recovery was not always performed at night to demonstrate that a large uptime can also be achieved with minimum human effort. Large gaps from MJD 58831 to MJD 58834 in the third campaign were caused by the shutdown of the air conditioners for facility maintenance. In the fourth campaign, a diode laser used in fiber comb 2 was broken, which caused a large downtime from MJD 58873 to MJD 58875. At MJD 58877, we stopped the clock operation and carried out a systematic evaluation of the microwave synthesis (See Section 5).

Figure 3 shows the distribution of interrupting events that occurred during the full campaign period. The number of interrupting events were counted according to the email alert history. We could basically link the email history to the types of

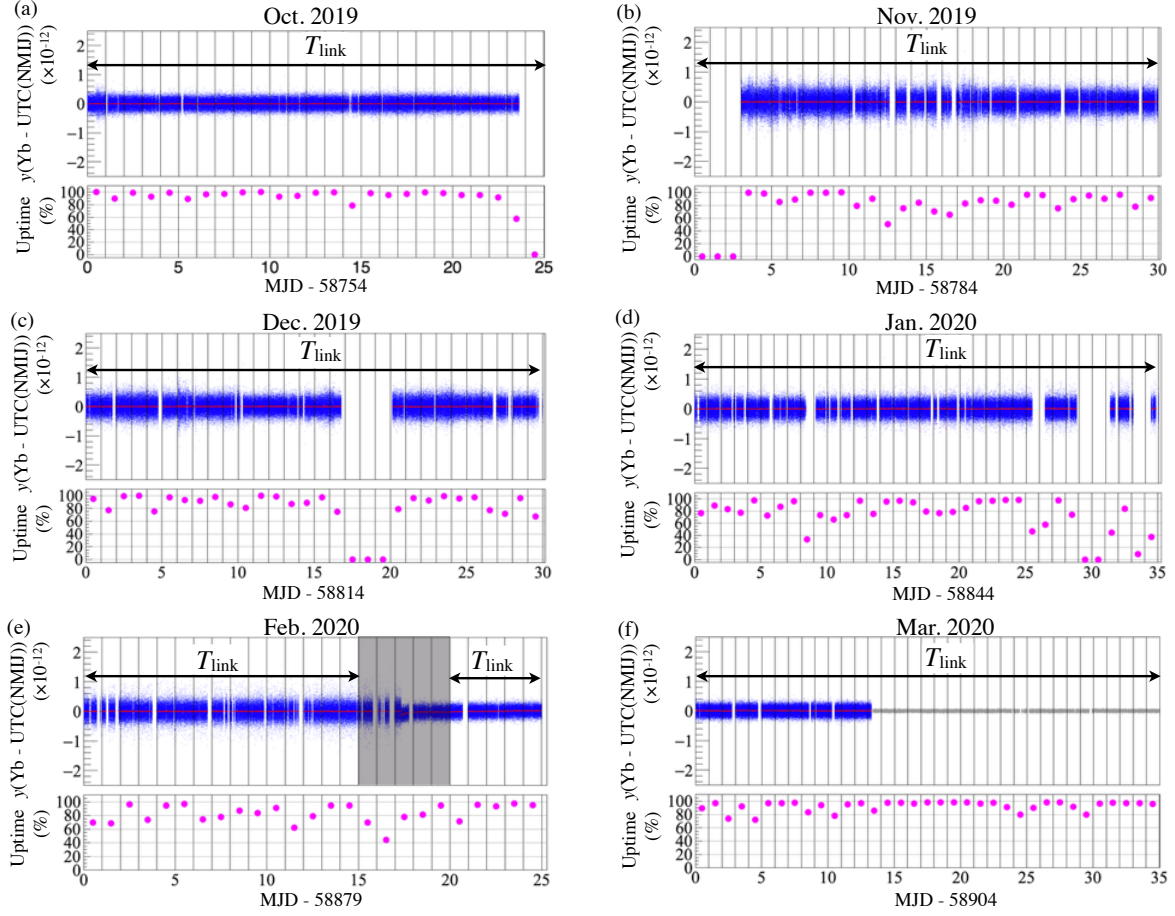


Figure 2. Fractional frequency of the Yb clock relative to UTC(NMIJ) ($y(\text{Yb} - \text{UTC}(\text{NMIJ}))$) and the uptime per day in the (a) first, (b) second, (c) third, (d) fourth, (e) fifth, and (f) sixth campaigns. The blue point corresponds to a 6.8 s average, the red point a 10^3 s average, and the gray point in (f) a 30 s average. T_{link} indicates the period employed to calculate the frequency difference between UTC(NMIJ) and TAI. The data in the shaded region in (e) were not used for the calculation due to a large excursion of the phase of UTC(NMIJ) at MJD 58896.

interruptions, but could not link some events due to a lack of records. These events are indicated by “No record” in Fig. 3. The clock operation was mostly interrupted by acoustic noise from a drainage pump in the facility (26% of the total number of interruptions), the instability of the injection locking (12%), mode hopping of the Ti:S laser (11%) and the 1156 nm ECDL (9%), and a small number of trapped atoms (8%). Earthquakes (6%) stopped the Yb clock mostly by dropping the lock of the 798 nm diode laser without implementing the relocking scheme. The other relockable light sources were resistant to small magnitude earthquakes. The other factors that interrupted the operation included rapid frequency drifts of the ULE cavity after the air conditioners were shutdown (MJD 58831 to MJD 58834) and temporary freezing of the data acquisition computer.

Figure 4 shows the number of interrupting events in each campaign. Most of the

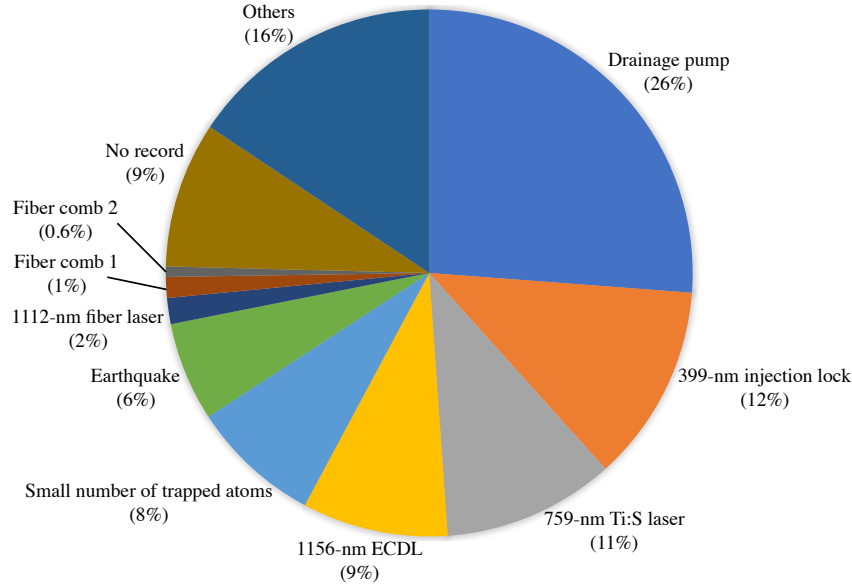


Figure 3. Distribution of interrupting events during the full campaign period.

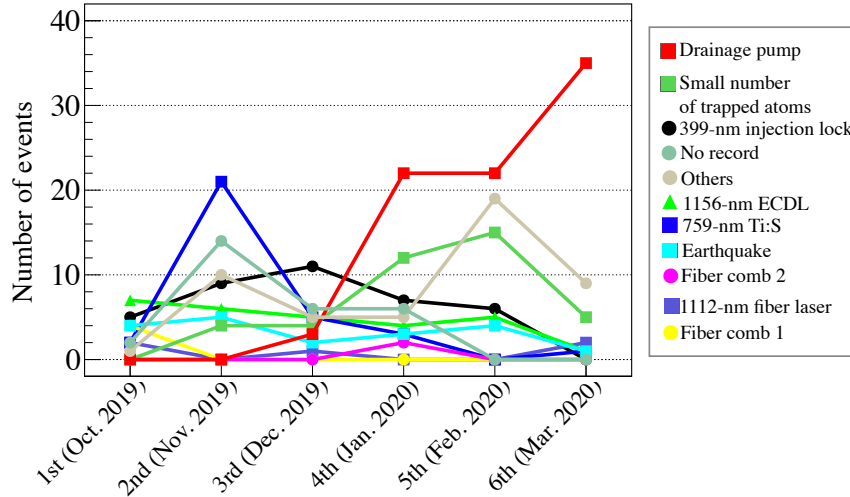


Figure 4. The number of interrupting events in each campaign.

interruptions occurred with a small number ($\lesssim 10$) in each campaign except for the Ti:S laser (blue square), a small number of trapped atoms (green square), and a drainage pump (red square). The lock of the Ti:S laser failed frequently especially in the second campaign. This problem was partially solved in the following campaigns by cleaning the mirrors used to introduce the pump laser beam and improving the signal-to-noise ratio of the error signal for the frequency locking to the comb. From the second campaign, the number of atoms trapped in the optical lattice gradually decreased (see Section 4), which increased the occurrence of lock failures. From the end of the third campaign, the Yb clock was frequently interrupted by a drainage pump, which had been installed in

the facility during the third campaign. The pump generated acoustic noise for about 30 minutes once a day when it drained water. During this period, the excitation probability of the atomic transition became almost zero due to the broadening of the clock laser linewidth.

4. Frequency stability and uncertainty of the optical lattice clock

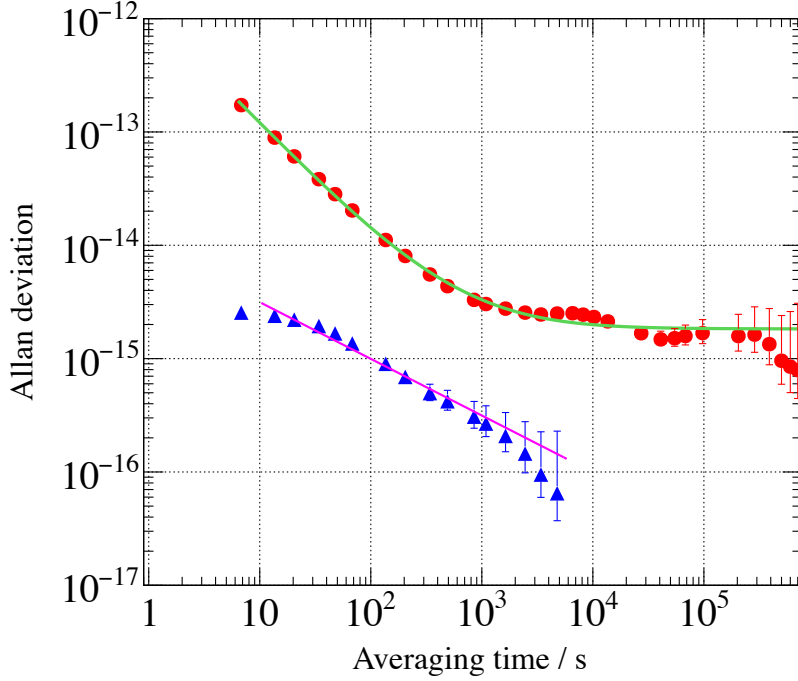


Figure 5. Allan deviation of UTC(NMIJ) referenced to the Yb clock (red dots) and the frequency ratio Yb/Sr (blue triangles). The green curve shows the stability of a simulated model of UTC(NMIJ) used to calculate the dead time uncertainty (see text). The purple line indicates a slope of $1.0 \times 10^{-14} / \sqrt{(\tau/s)}$.

We evaluated the frequency stability of the Yb optical lattice clock by comparing it with our Sr optical lattice clock [43]. Figure 5 shows the Allan deviation of the frequency ratio Yb/Sr, which was improved with a slope of $1.0 \times 10^{-14} / \sqrt{(\tau/s)}$ and reached low 10^{-16} in several thousand seconds. Figure 5 also shows the frequency stability of UTC(NMIJ) relative to the Yb clock, which was calculated from the data of the first campaign (see Fig. 2 (a)). During this campaign period, the frequency offset of the auxiliary output generator for UTC(NMIJ) was constant.

Table 2 lists the systematic shifts and uncertainties of the Yb optical lattice clock obtained in the first campaign. The uncertainty evaluation is mostly based on our previous evaluation [35]. The density shift and the servo error differed slightly depending on the data obtained in each campaign.

The lattice induced light shift was estimated using a model [44–46] that includes the contributions from the dominant electric-dipole ($E1$) polarizability, the multipolar ($M1$

Table 2. Systematic shifts and uncertainties of the ^{171}Yb optical lattice clock obtained in the first campaign from MJD 58754 to MJD 58778.

Effect	Shift ($\times 10^{-17}$)	Uncertainty ($\times 10^{-17}$)
Lattice light	3.4	33.1
BBR	-263.8	20.8
Density	-8.3	6.4
Second-order Zeeman	-5.2	0.3
Probe light	0.4	0.2
Servo error	-4.7	1.1
AOM switching	—	1
Total	-278.3	39.6

and $E2$) polarizability, and hyperpolarizability [47]. To calculate the shift using this model, the effective trap potential depth V_e , which is less than the maximum trap depth $V_0 = 450E_r$ due to the radial motion of the atoms, and the average vibrational quantum number $\langle n \rangle$ were estimated by sideband spectroscopy of the clock transition [48]. The obtained values were $V_e = 342(28)E_r$ and $\langle n \rangle = 2.1(6)$. The frequency of the lattice laser was stabilized at $\nu_1 = 394\,798\,263$ MHz.

To find the $E1$ polarizability coefficient a and the $E1$ magic frequency ν_{E1} , we have previously measured the light shift as a function of the frequency of the lattice laser [35], and fitted the obtained data with the light shift model [45]. To estimate the variation of a and ν_E resulting from the systematic uncertainty of the fixed parameters in the light shift model (V_e , $\langle n \rangle$, and the multipolar and hyperpolarizability shifts), we have employed a Monte Carlo method in which the fittings were repeated with different permutations of the fixed parameters. Since the distribution of a obtained from many fittings was asymmetric and had a very long tail mainly due to a relatively large uncertainty in our estimation of V_e , we have previously calculated a mean value of a by removing rare events in the tail. Here, we employed a value of a that was determined with center values of the fixed parameters. The uncertainty of a was estimated from a 68% coverage interval of the distribution of a . The same method was applied to the estimation of ν_{E1} . We obtained $a = 0.020(13)$ mHz/(MHz E_r) and $\nu_{E1} = 394\,798\,244(25)$ MHz, which agreed with our previous estimation [35] and the values reported by other groups [20, 46, 47, 49]. Finally, the light shift was estimated to be $3.4(33.1) \times 10^{-17}$ with a , ν_{E1} , ν_1 , $\langle n \rangle$, V_e estimated here, and the sensitively coefficients for the multipolar and hyperpolarizability shifts used in our previous evaluation [35].

The blackbody radiation (BBR) shift was estimated to be $-263.8(20.8) \times 10^{-17}$, which includes the contribution from the vacuum chamber and the atomic oven considered in our previous evaluation [35] and also that from the newly-installed heated window at 204°C. To include this new contribution, the BBR shift induced by the

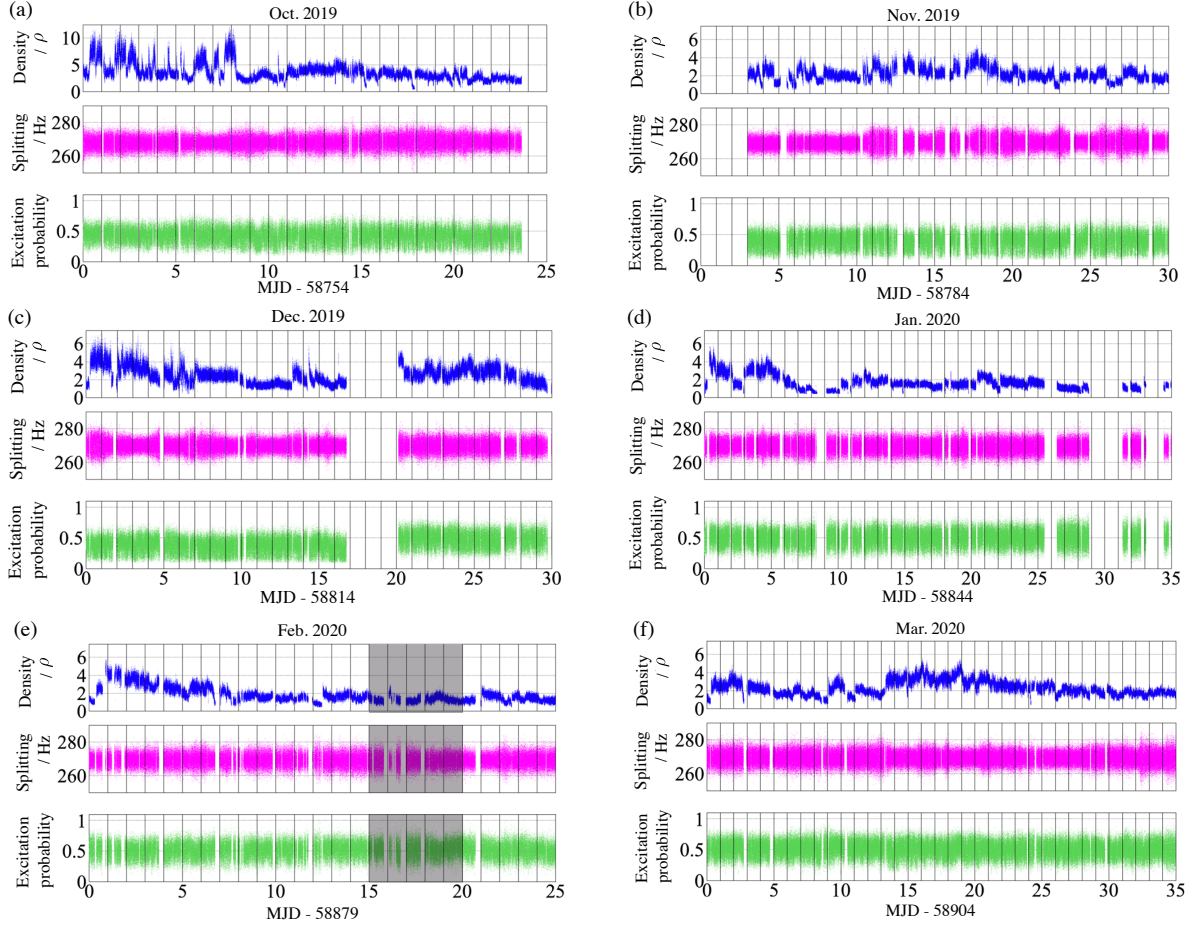


Figure 6. Atomic density ($\rho \sim 10^{14} \text{ m}^{-3}$) in the optical lattice (blue points), Zeeman splitting (pink points), excitation probability (green points) in the (a) first, (b) second, (c) third, (d) fourth, (e) fifth, and (f) sixth campaigns. The data point corresponds to a 6.8 s average. Some of the data at MJD 58789 in (b) were not recorded. The data in the shaded region (MJD 58894 to MJD 58899 in (e)) were not used for the systematic evaluation. The fiber for the 399 nm light was replaced at MJD 58794 in (b), MJD 58814 in (c), MJD 58879 in (e), and MJD 58917 in (f). The 1112 nm semiconductor amplifier was replaced at MJD 58844 in (d), MJD 58853 in (d), MJD 58891 in (e), and MJD 58913 in (f).

heated window was calculated using a model [50] in which the atoms are located at the center of a stainless-steel sphere with an emissivity of 0.1. The radius of the sphere is equal to the distance between the atoms and the heated window ($\sim 140 \text{ mm}$). The BBR photons at 204°C are provided from a small portion of the sphere's surface with its area equal to that of the heated window seen by the atoms ($\sim 260 \text{ mm}^2$). This model takes into account the diffuse reflection of the BBR photons on the stainless-steel wall, which increases the effective solid angle by a factor of ~ 10 compared with the geometric solid angle. With the sensitivity coefficient [51, 52], the calculated shift due to the heated window was -1.8×10^{-16} . This shift value was also conservatively taken as an uncertainty.

The density shift was estimated from the atomic density in each campaign. The blue points in Fig. 6 show the atomic density data. The density decreased with a time scale of ~ 10 days largely due to a reduction in the transmission efficiency of the 399 nm light through the optical fiber and the output power of the 1112 nm semiconductor amplifier. Some of these components were replaced (see the caption of Fig. 6) when we could not keep the stabilization of the clock laser to the atomic transition. The status of the stabilization was confirmed by monitoring the Zeeman splittings and the excitation probabilities (see pink and green points in Fig. 6). The short-term (a few days) fluctuation of the density was mainly caused by variations in the spectral purity of the injection locking, the polarization rotation of the cooling lasers through the optical fiber, and pointing instabilities of the cooling beam at 399 nm induced by an AOM or a damaged optical fiber. In the first campaign (see blue points in Fig. 6 (a)), the mean value of the atomic density was $3.6(1.6)\rho$ with $\rho \sim 10^{14} \text{ m}^{-3}$. The uncertainty of 1.6ρ was estimated from the standard deviation. We also added an uncertainty of $\sim 10\%$ to the estimation of the density according to the fluctuation of the 399 nm probe power. With our sensitivity coefficient [35] and a scaling of the trap volume with $V_0^{-3/2}$ [3], the shifts were determined as $-8.3(6.4) \times 10^{-17}$, $-4.9(3.4) \times 10^{-17}$, $-5.7(4.1) \times 10^{-17}$, $-3.9(3.0) \times 10^{-17}$, $-4.5(3.5) \times 10^{-17}$, and $-5.3(3.7) \times 10^{-17}$ in the first, second, third, fourth, fifth, and sixth campaigns, respectively. We observed that the mean excitation probability changed from 0.42 to 0.50 after the air conditioners were shutdown (MJD 58831 to MJD 58834) (see Fig. 6 (c)). We attributed this to a variation of the spin-polarization efficiency due to a large frequency change of the ULE cavity. This can change the shift coefficient, since the density shift depends on (i) the excitation probability mostly due to the p -wave interaction [53–55] and (ii) the impurity of the spin-polarization [4, 54]. Based on the measured results of Ref. [54], we estimated that in our relatively low atomic density, the change due to those effects is negligibly small compared with the uncertainty in our evaluation.

The second-order Zeeman shift was estimated from the Zeeman splitting measured in each campaign (see pink points in Fig. 6). In the first campaign, the mean value of the splitting was 268(3) Hz, where the uncertainty was estimated from the standard deviation. The shift was found to be $-5.2(3) \times 10^{-17}$ using our sensitivity coefficient [35]. The mean splitting value was almost constant (268 - 270 Hz) during the entire campaign period.

The probe light shift was calculated to be $4(2) \times 10^{-18}$ from the shift value of Ref. [4] and the fact that the laser intensity adjusted for the π pulse was inversely proportional to the time duration of the pulse.

The servo error was estimated by averaging the differences between the excitation probabilities of the high- and low-spectral shoulders for the data obtained in each measurement campaign. The servo errors were estimated to be $-4.7(1.1) \times 10^{-17}$, $-4.8(1.0) \times 10^{-17}$, $4.6(10.8) \times 10^{-17}$, $-2.8(1.2) \times 10^{-17}$, $-6.0(0.9) \times 10^{-17}$, and $-4.1(1.4) \times 10^{-17}$ in the first, second, third, fourth, fifth, and sixth campaigns, respectively. The relatively large uncertainty of 10.8×10^{-17} in the third campaign arose from the rapid

frequency drifts of the ULE cavity after the air conditioners were shutdown (MJD 58831 to MJD 58834).

5. Uncertainty of the frequency comparison by the comb

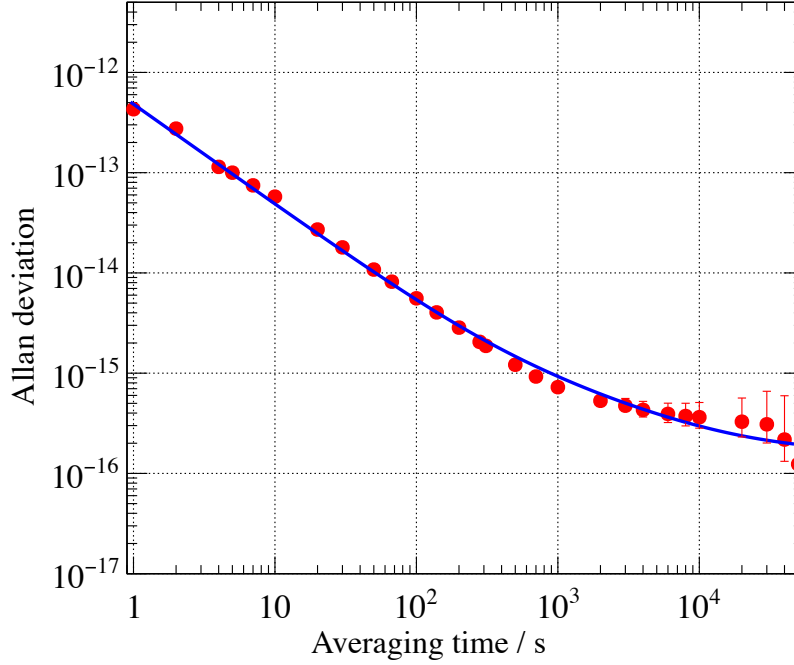


Figure 7. Allan deviation calculated from the frequency difference between two independent combs except for the reference signal of UTC(NMIJ). The blue curve indicates the fit of a function which includes the white phase, the white frequency, and the flicker frequency noise components.

To evaluate the uncertainty of the comb-based frequency comparison between the Yb clock and UTC(NMIJ), we compared fiber comb 2 (see Fig. 1) with another comb (fiber comb 3, not shown in Fig. 1) that was independent except for the 10 MHz reference signal of UTC(NMIJ). These combs had independent setups for the microwave synthesis including the 90-fold frequency multiplication. We simultaneously measured the frequency of an acetylene-stabilized laser at $1.5 \mu\text{m}$ against UTC(NMIJ) by using these two combs, and calculated the frequency difference between the combs. In the first measurement from MJD 58712 to MJD 58713, the fractional frequency difference (fiber comb 2 - fiber comb 3) was found to be 9.7×10^{-17} , which was the average of the frequency difference data obtained for $\sim 10^5$ s. Figure 7 shows the Allan deviation calculated from the frequency difference data. The Allan deviation is likely limited by a flicker floor of low 10^{-16} at averaging times $\tau \geq 10^4$ s. By fitting the Allan deviation with a function which includes the white phase, the white frequency, and the flicker frequency noise components, the flicker component was estimated to be 1.6×10^{-16} . In the second measurement at MJD 58877, the frequency difference and the flicker component were

-1.1×10^{-16} and 4.5×10^{-16} , respectively. We took an average of the two flicker noise values (3.1×10^{-16}) and divided it by $\sqrt{2}$. The obtained value 2.2×10^{-16} was adopted as an uncertainty of the frequency comparison. Previous optical-optical comparisons [56] have shown that the uncertainty resulting from the comb itself is negligibly small. We also carried out another measurement in which the two combs shared the common frequency multiplier, and observed that the Allan deviation was improved with a τ^{-1} slope for $\tau > 10^3$ s. Thus, we attributed the flicker noise mainly to the frequency multiplier.

6. Absolute frequency measurement

Since UTC(NMIJ) was continuously compared with TAI via a satellite link (see Fig. 1), the frequency of the Yb clock referenced to the SI second $y(\text{Yb} - \text{SI})$ can be deduced from the data $y(\text{Yb} - \text{UTC}(\text{NMIJ}))$ in Fig. 2 by the relationship,

$$\begin{aligned} y(\text{Yb} - \text{SI}) &= y(\text{Yb} - \text{UTC}(\text{NMIJ})) \\ &\quad + y(\text{UTC}(\text{NMIJ}) - \text{TAI}) \\ &\quad + y(\text{TAI} - \text{SI}), \end{aligned} \tag{2}$$

where $y(\text{UTC}(\text{NMIJ}) - \text{TAI})$ and $y(\text{TAI} - \text{SI})$ denote the fractional frequency differences between (i) UTC(NMIJ) and TAI and (ii) TAI and SI, respectively. These values are provided in Circular T [57], which is a monthly report issued by BIPM. Since BIPM only computes $y(\text{UTC}(\text{NMIJ}) - \text{TAI})$ for 5-day intervals, we chose a 25-day period (MJD 58754 - MJD 58779), a 30-day period (MJD 58784 - MJD 58814), a 30-day period (MJD 58814 - MJD 58844), a 35-day period (MJD 58844 - MJD 58879), a 20-day period (MJD 58879 - MJD 58884 and MJD 58899 - MJD 58904), and a 35-day period (MJD 58904 - MJD 58939) for the first - sixth campaigns, respectively, to calculate the average value of $y(\text{UTC}(\text{NMIJ}) - \text{TAI})$. These periods are indicated by T_{link} in Fig. 2. In the fifth campaign, a 5-day period from MJD 58894 to MJD 58899 (see the shaded region of Fig. 2 (e)) was excluded, since a large excursion of the phase of UTC(NMIJ) occurred during maintenance of the hydrogen maser at MJD 58896. Figure 8 shows the $y(\text{Yb} - \text{SI})$ value obtained for each campaign.

The choice of the period T_{link} causes an uncertainty due to the dead time in the comparison of the Yb clock and UTC(NMIJ). This dead time uncertainty was calculated by using a numerical simulation described in Ref. [58]. The simulation generated time series data of the frequency according to the noise characteristics: $1 \times 10^{-12}/(\tau/\text{s})$ for the white phase modulation, $7 \times 10^{-14}/\sqrt{(\tau/\text{s})}$ for the white frequency modulation (FM), 2×10^{-15} for the flicker FM, and $4 \times 10^{-24}\sqrt{(\tau/\text{s})}$ for the random walk FM. These noise parameters were chosen to reproduce the typical stability of UTC(NMIJ) (see green curve in Fig. 5). We generated two hundred time series patterns and calculated the standard deviation between the frequency averaged over the entire 25-, 30-, or 35-day period and the mean frequency for the time during which the Yb clock was operated. This standard deviation corresponds to the dead time uncertainty. The dead

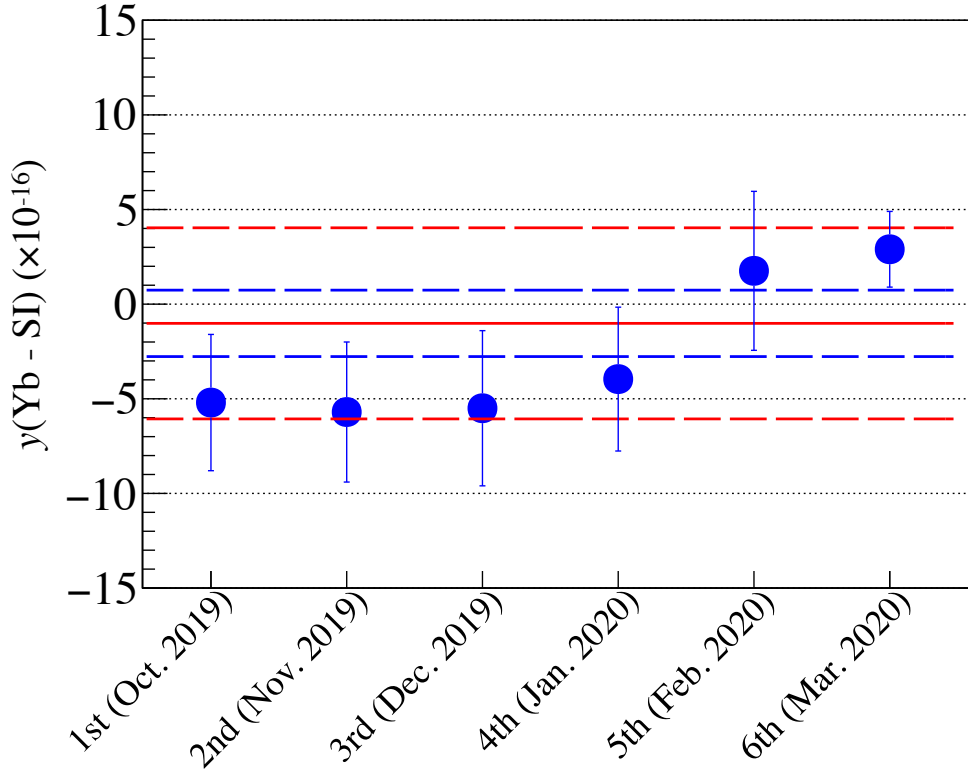


Figure 8. Fractional frequency of the Yb clock referenced to the SI second ($y(\text{Yb} - \text{SI})$) obtained in each campaign. The error bar is given by the total statistical uncertainty for each campaign. The solid red line indicates the weighted mean, the dashed blue lines indicate the total statistical uncertainty in the full period, and the dashed red lines indicate the total uncertainty including the systematic uncertainties.

time uncertainties were estimated as 2.0×10^{-16} , 3.0×10^{-16} , 3.3×10^{-16} , 3.3×10^{-16} , 1.1×10^{-16} , and 8×10^{-17} for the first, second, third, fourth, fifth, and sixth campaigns, respectively. A frequency correction arose from the dead time when the frequency steering of UTC(NMIJ) was carried out. We added corrections of $-9.9(2) \times 10^{-18}$, $-1.0(9) \times 10^{-16}$, and $7.9(5) \times 10^{-17}$ in the third, fifth, and sixth campaigns, respectively.

In addition, the uncertainty resulting from the dead time when we compare TAI and SI arises from the fact that BIPM calculates the $y(\text{TAI} - \text{SI})$ value based on an evaluation with primary and secondary frequency standards for 25, 30, or 35 days, whereas our measurement period T_{link} did not fully cover the evaluation period of BIPM in the first and fifth campaigns. This uncertainty was estimated to be 1.6×10^{-16} in the first campaign, and 4×10^{-17} in the full period based on the stability of the Echelle Atomique Libre (EAL) given in Circular T: $1 \times 10^{-15} / \sqrt{(\tau/\text{day})}$ for the white FM, 0.35×10^{-15} for the flicker FM, and $0.2 \times 10^{-16} \sqrt{(\tau/\text{day})}$ for the random walk FM.

The satellite link uncertainty in $y(\text{UTC}(\text{NMIJ}) - \text{TAI})$ was calculated to be 2.3×10^{-15} for $T_{\text{link}} = 25$ days, 2.0×10^{-16} for $T_{\text{link}} = 30$ days, and 1.7×10^{-16} for $T_{\text{link}} = 35$ days using the recommended formula $(\sqrt{2}u_A)/[(3600 \times 24 \times 5)(\frac{T_{\text{link}}}{5})^{0.9}]$ [16] with the statistical uncertainty $u_A = 0.3$ ns reported in Circular T.

Table 3. Uncertainty budget for the absolute frequency measurement of the ^{171}Yb clock transition.

Effect	First campaign ($\times 10^{-16}$)	Full period ($\times 10^{-16}$)
Statistics		
Yb	0.07	0.03
Dead time in Yb - UTC(NMIJ)	2.0	0.6
Dead time in TAI - SI	1.6	0.4
UTC(NMJI) - TAI satellite link	2.3	0.8
TAI - SI	0.9	0.4
Statistics total	3.6	1.8
Systematics		
Yb	4.0	4.0
Microwave synthesis	2.2	2.2
TAI - SI	1.1	1.1
Gravitational red shift	0.6	0.6
Systematics total	4.7	4.7
Total	5.9	5.0

The statistical and systematic uncertainties of $y(\text{TAI} - \text{SI})$ were calculated from the total uncertainty of $y(\text{TAI} - \text{SI})$ and the systematic uncertainties of the primary and secondary frequency standards reported in Circular T. During the present half-year period, the frequency of TAI was calibrated by using the following frequency standards: Cs thermal beam clocks (PTB-Cs1 and PTB-Cs2 [59]), Cs fountain clocks (SYRTE-FO1, SYRTE-FO2, SYRTE-FOM [60], PTB-CSF1, PTB-CSF2 [61], SU-CsFO2 [62], and NIM5 [63]), a Rb fountain clock (SYRTE-FORb [64]), and a Sr optical lattice clock (NICT-Sr1 [29]). Since Circular T only provides the total uncertainty of $y(\text{TAI} - \text{SI})$, the systematic uncertainty of $y(\text{TAI} - \text{SI})$ was estimated using the systematic uncertainties and weights of the individual frequency standards based on a method described in Ref. [65]. The estimated systematic uncertainty of $y(\text{TAI} - \text{SI})$ changed between 1.1×10^{-16} and 1.2×10^{-16} during the half year period. We adopted an average value of 1.1×10^{-16} for the full campaign period. The statistical uncertainty of $y(\text{TAI} - \text{SI})$ was calculated with the above systematic uncertainty to reproduce the total uncertainty given in Circular T. The statistical uncertainty ranged between 0.8×10^{-16} and 1.5×10^{-16} , and decreased to 4×10^{-17} in the full campaign period.

Table 3 summarizes the uncertainties for the absolute frequency measurement. The statistical uncertainty of the Yb clock was calculated using the stability of the Yb/Sr ratio measurement (see Fig. 5) with the duration of the operation. The gravitational red shift was estimated to be $22.9(6) \times 10^{-16}$ using the Yb height from the conventionally adopted geoid potential ($62\,636\,856.0 \text{ m}^2/\text{s}^2$). The total statistical uncertainty in the

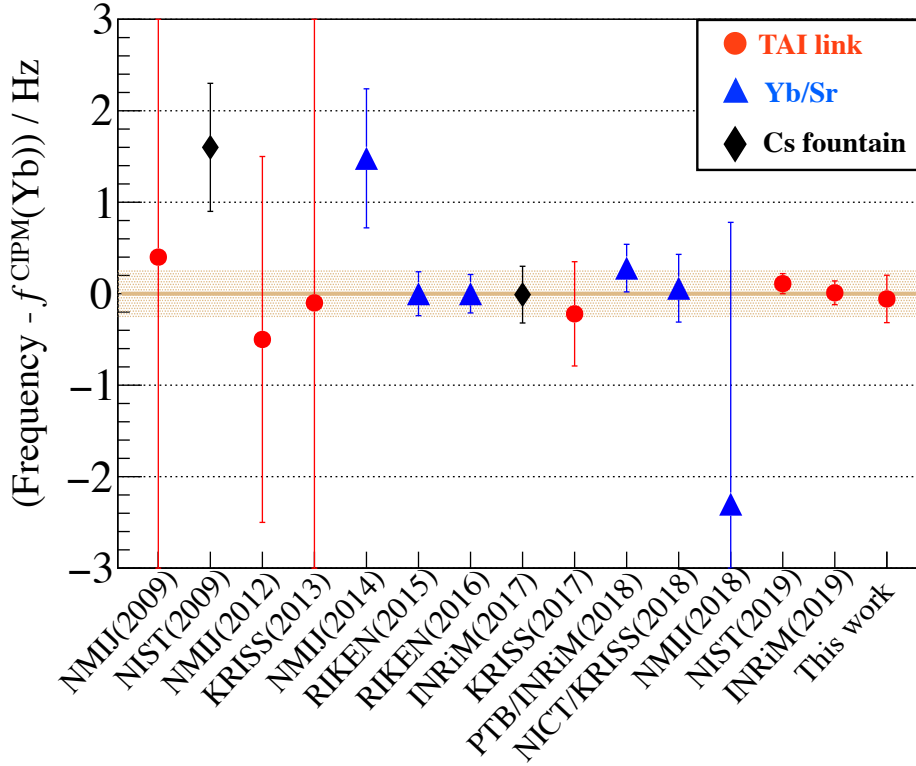


Figure 9. Absolute frequencies of the ^{171}Yb clock transition using a link to TAI [19, 20, 49, 66–68] (red circles), the $^{171}\text{Yb}/^{87}\text{Sr}$ frequency ratio [28, 45, 69–72] and the CIPM recommended frequency of ^{87}Sr [8] (blue triangles), and local Cs fountain clocks [11, 15] (black diamonds). The shaded region indicates the CIPM recommended value of ^{171}Yb and $f^{\text{CIPM}}(\text{Yb}) = 518\,295\,836\,590\,863.6(26)$ Hz [8]. NIST: National Institute of Standards and Technology, KRISS: Korea Research Institute of Standards and Science, INRiM: Istituto Nazionale di Ricerca Metrologica, PTB: Physikalisch-Technische Bundesanstalt, NICT: National Institute of Information and Communications Technology.

full period was 1.8×10^{-16} (dashed blue lines in Fig. 8), which was obtained by inflating the uncertainty of the weighted mean by the square root of the reduced chi-square $\sqrt{\chi_{\text{red}}^2} = 1.3$. Finally, we obtained $y(\text{Yb} - \text{SI}) = -1.1(5.0) \times 10^{-16}$. The absolute frequency of the Yb clock transition was determined as $518\,295\,836\,590\,863.54(26)$ Hz. The total uncertainty was mostly limited by the systematic uncertainties of the Yb clock and the microwave synthesis. Our determined value agreed with the recommended frequency $f^{\text{CIPM}}(\text{Yb})$ and the results of previous measurements by many groups (see Fig. 9).

7. Discussions and conclusion

The uncertainty in the link between the Yb clock and the SI second was 2.4×10^{-16} , which was calculated by using the quadratic sum of the uncertainties due to the dead times in both Yb - UTC(NMIJ) and TAI - SI, the satellite link, and the microwave

synthesis. The reduction of the link uncertainty by the continuous operation also enables measurements of the frequency ratios at the 10^{-16} level between remotely-located secondary representations of the second. For example, during the present half-year period, a Rb fountain clock (SYRTE FORb) [64] was running. The frequency difference data $y(\text{TAI} - \text{Rb})$ for 180 days were obtained from Circular T. With our data $y(\text{Yb} - \text{TAI})$, we determined the Yb/Rb ratio as 75 833.197 545 114 174(42) with a relative uncertainty of 5.5×10^{-16} . This agreed with the ratio calculated from the recommended frequencies $f^{\text{CIPM}}(\text{Yb})/f^{\text{CIPM}}(\text{Rb}) = 75\,833.197\,545\,114\,196(59)$ [8] and the value 75 833.197 545 114 192(33) reported by another group [19]. As another example, a Sr optical lattice clock (NICT-Sr1 [29]) calibrated the TAI frequency for 20 days during the sixth campaign period. This enabled us to determine the Yb/Sr ratio as 1.207 507 039 343 337 82(75) with a fractional uncertainty of 6.2×10^{-16} . This was in agreement with the most accurate previous value 1.207 507 039 343 337 749(55) [45] and the other values with uncertainties at the 10^{-16} level [20, 28, 70, 71].

The expectation value of the uptime of the Yb clock was calculated under the condition where the Yb clock is fully unattended during a night interval of 8 hours, and where long downtimes resulting from rare events such as facility maintenance are not included. The number of interrupting events that required manual recovery was 580 during the full campaign period. This was obtained by counting the number of time gaps of more than 1 minute in the frequency data (Fig. 2). Since the Yb clock was operated with a 80.3% uptime for 185 days, the mean number of interruptions per hour was $580/(0.803 \times 185 \times 24 \text{ hours}) = 0.16/\text{hour}$. To estimate the probability of the occurrence of n interrupting events in an interval of T hours, we employed a Poisson distribution,

$$P(n, T) = \frac{(0.16T)^n e^{-0.16T}}{n!}. \quad (3)$$

To calculate the expected uptime, the typical time for manually restarting the operation is needed. Figure 10 shows a histogram of the recovery time, which was obtained from time gaps in the frequency data (Fig. 2). Excluding long gaps exceeding half a day, the mean recovery time was 0.72 hours. The expected dead time during a 16-hour period of human work was then calculated as $\sum_{n=0}^{\infty} nP(n, 16) \times 0.72 \text{ hours} = 1.8 \text{ hours}$. During an 8-hour night period, the operation is stopped after one interrupting event. In this case, the expected dead time is calculated as $\int_0^8 \frac{d(1-P(0, T))}{dT} (8 - T) dT = 3.5 \text{ hours}$. The uptime per day was therefore expected to be 78%.

To consider the optimum conditions for the operation, we carried out a simulation of the dead time uncertainty as a function of the clock uptime (see Figure 11). In this simulation, the dead time was homogeneously distributed for a 30-day period, except for a large time gap of $T_{\text{gap}} = 1 - 5$ days in the middle of the period. Without the large gap (indicated as “None” in Fig. 11), the dead time uncertainty falls below 10^{-16} for uptimes of $\geq 80\%$. When the clock operation is stopped for $T_{\text{gap}} = 1 - 5$ days, the uncertainty no longer reaches below 10^{-16} even though the uptime for the overall period is $\geq 80\%$. This indicates that the uncertainties calculated with the actual duration of

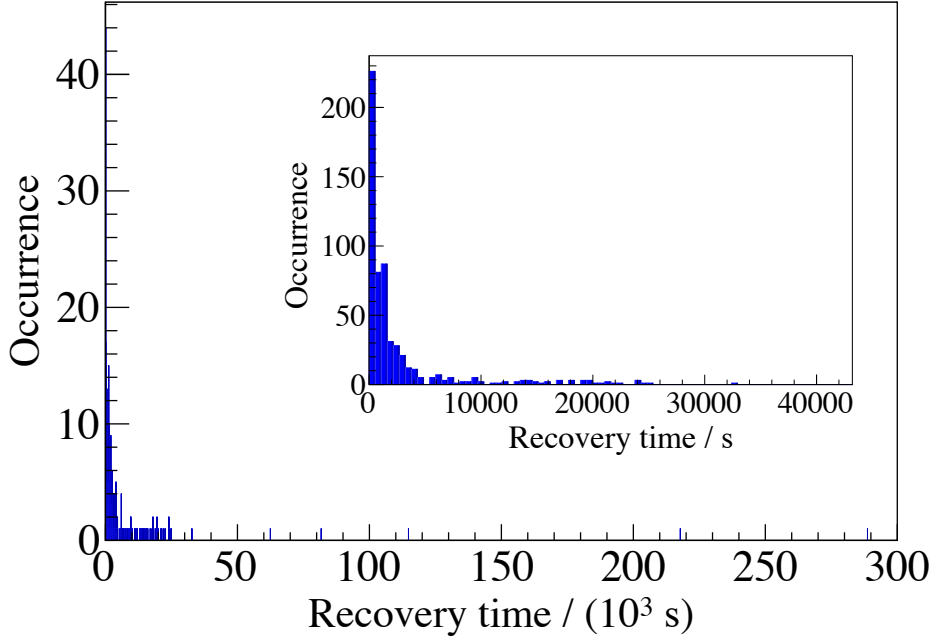


Figure 10. Histogram of the recovery time of more than 1 minute. The inset shows recovery times within half a day with a different bin size, from which the mean recovery time was obtained as 0.72 hours.

the clock operation are mostly determined by the instabilities of UTC(NMIJ) during the large gaps. When we take into account the fact that the uncertainty of the absolute frequency measurement is limited by the systematic uncertainties of the Yb clock and the microwave synthesis (the combined uncertainty is 4.6×10^{-16}), it may be enough to reduce the dead time uncertainty to $\sim 2 \times 10^{-16}$. In this case, the optimum condition is to operate the clock every day with a moderate uptime of $\sim 50\%$. This is well below our expectation value of the uptime (78%, see above). It should be noted that daily repetition of the startup and shutdown of the clock increases human effort, and thus it is better in practice to let the clock run continuously.

Previous studies have demonstrated an improvement in local timescales by steering flywheel oscillators to intermittently operated lattice clocks [13, 29–31]. In these methods, the stabilities of the timescales are limited by the fluctuations of the flywheels during the dead time of the clocks, and thus can be further improved by continuous operation. An analysis for our local timescale will be presented in a future publication.

The performance at the present level can make a significant contribution to the search for new physics. For example, local position invariance has been tested by looking for an annual variation of the gravitational red shift of atomic clocks [12, 19, 22]. As demonstrated in previous experiments that utilized continuously running fountain clocks and hydrogen masers [73], the continuous operation contributes to reduce the statistical uncertainty in a relatively short term, resulting in a stringent limit on violation of local position invariance. In our case, this experiment can be carried out by comparing the Yb clock with a local Cs fountain clock [74] or a hydrogen maser. Another example is

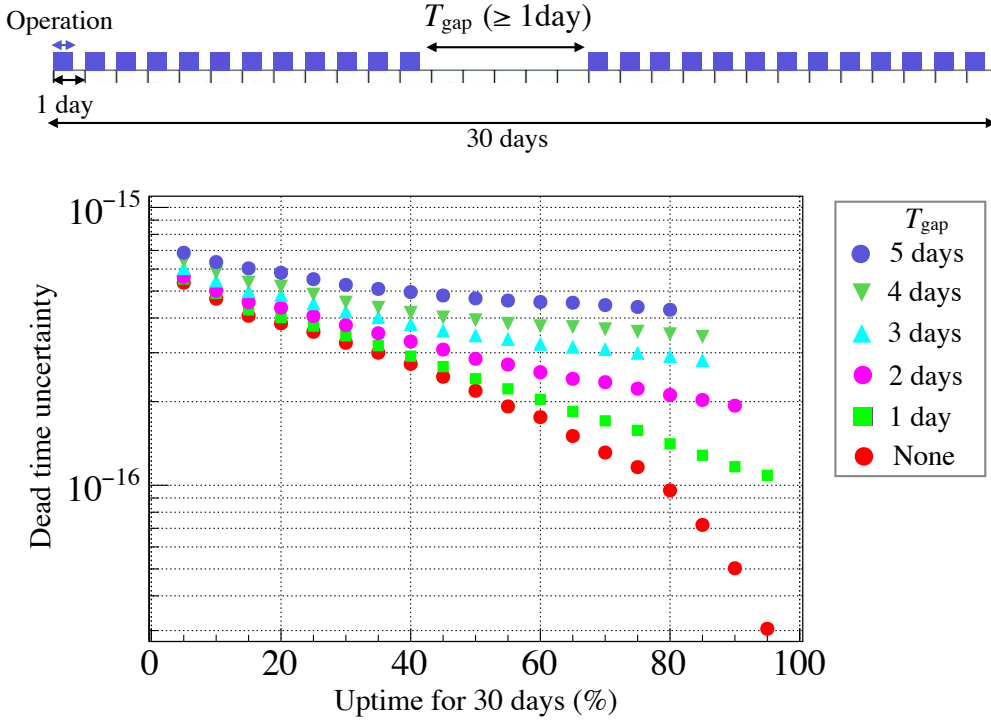


Figure 11. Simulated dead time uncertainty as a function of the clock uptime for 30 days. As shown in the top figure, the dead time is homogeneously distributed over the 30-day period, except for a large gap time of $T_{\text{gap}} = 1 - 5$ days in the middle of the period.

that transient variations of the fine structure constant resulting from the passage of dark matter may be observed in a global network of optical clocks [24]. The detection of the transient effects relies on correlations in the frequency data of worldwide clocks running simultaneously [75]. To obtain a large amount of temporally overlapped data from laboratories worldwide, it is highly desirable that the participating clocks are capable of running continuously for a long period. The continuous operation also makes it possible to search for dark matter interactions on long timescales that could not be studied in previous experiments [75, 76].

In conclusion, we have demonstrated the nearly continuous operation of an Yb optical lattice clock with an uptime of 80.3% for half a year. This enabled us to link the Yb clock to the SI second with an uncertainty of 2.4×10^{-16} , and to determine the absolute frequency of the Yb clock transition with a total uncertainty of 5.0×10^{-16} . The present performance preliminary demonstrated that the robustness of optical lattice clocks can reach a level comparable to that of Cs fountain clocks. This work constitutes an important step towards the redefinition of the SI second.

Acknowledgments

We thank H. Katori, M. Takamoto, and H. Imai for providing information on their vacuum systems, and S. Okubo for technical assistance. We are indebted to national metrology institutes for their efforts in operating the primary and secondary frequency standards and making the data available in Circular T. This work was supported by Japan Society for the Promotion of Science (JSPS) KAKENHI Grant Number 17H01151, and 17K14367, and JST-Mirai Program Grant Number JPMJMI18A1, Japan.

Reference

- [1] Bloom B J, Nicholson T L, Williams J R, Campbell S L, Bishof M, Zhang X, Zhang W, Bromley S L, and Ye J 2014 An optical lattice clock with accuracy and stability at the 10^{-18} level *Nature* **506** 71-75
- [2] Ushijima I, Takamoto M, Das M, Ohkubo T, and Katori H 2015 Cryogenic optical lattice clocks *Nat. Photon.* **6** 185-189
- [3] Nicholson T L, Campbell S L, Hutson R B, Marti G E, Bloom B J, McNally R L, Zhang W, Barrett M D, Safronova M S, Strouse G F, Tew W L, and Ye J 2015 Systematic evaluation of an atomic clock at 2×10^{-18} total uncertainty *Nat. Commun.* **6** 6896
- [4] McGrew W F, Zhang X, Fasano R J, Schäffer S A, Beloy K, Nicolodi D, Brown R C, Hinkley N, Milani G, Schioppo M, Yoon T H, and Ludlow A D 2018 Atomic clock performance enabling geodesy below the centimetre level *Nature* **564** 87-90
- [5] Bothwell T, Kedar D, Oelker E, Robinson J M, Bromley S L, Tew W L, Ye J, and Kennedy C J 2019 JILA SrI optical lattice clock with uncertainty of 2.0×10^{-18} *Metrologia* **56** 066004.
- [6] Gill P 2011 When should we change the definition of the second? *Philos. Trans. Roy. Soc. A* **369** 4109-4130
- [7] Hong F-L 2016 Optical frequency standards for time and length applications *Meas. Sci. Technol.* **28** 012002
- [8] Riehle F, Gill P, Arias F, and Robertsson L. 2018 The CIPM list of recommended frequency standard values: Guidelines and procedures *Metrologia* **55** 188-200
- [9] Lodewyck J 2019 On a definition of the SI second with a set of optical clock transitions *Metrologia* **56** 055009
- [10] Campbell G K, Ludlow A D, Blatt S, Thomsen J W, Martin M J, de Miranda M H G, Zelevinsky T, Boyd M M, Ye J, Diddams S A, Heavner T P, Parker T E, and Jefferts S R 2008 The absolute frequency of the 87Sr optical clock transition *Metrologia* **45** 539-548
- [11] Lemke N D, Ludlow A D, Barber Z W, Fortier T M, Diddams S A, Jiang Y, Jefferts S R, Heavner T P, Parker T E, and Oates C W 2009 Spin-1/2 optical lattice clock *Phys. Rev. Lett.* **103** 063001
- [12] Le Targat R, Lorini L, Le Coq Y, Zawada M, Gueña J, Abgrall M, Gurov M, Rosenbusch P, Rovera D G, Nagórny B, Gartman R, Westergaard P G, Tobar M E, Lours M, Santarelli G, Clairon A, Bize S, Laurent P, Lemonde P, and Lodewyck J 2013 Experimental realization of an optical second with strontium lattice clocks *Nat. Commun.* **4** 2109
- [13] Grebing C, Al-Masoudi A, Dörsher S, Häfner S, Gerginov V, Weyers S, Lipphardt B, Riehle F, Sterr U, and Lisdat C 2016 Realization of a timescale with an accurate optical lattice clock *Optica* **3** 563-569
- [14] Lodewyck J, Bilicki S, Bookjans E, Robyr J-L, Shi C, Vallet G, Le Targat R, Nicolodi D, Coq Y, Guéna J, Abgrall M, Rosenbusch P, and Bize S 2016 Optical to microwave clock frequency ratios with a nearly continuous strontium optical lattice clock *Metrologia* **53** 1123-1130
- [15] Pizzocaro M, Thoumany P, Rauf B, Bregolin F, Milani G, Clivati C, Costanzo G A, Levi F, and Calonico D 2017 Absolute frequency measurement of the $^1\text{S}_0 - ^3\text{P}_0$ transition of ^{171}Yb *Metrologia* **54** 102-112

- [16] Panfilo G and Parker T E 2010 A theoretical and experimental analysis of frequency transfer uncertainty, including frequency transfer into TAI *Metrologia* **47** 552-560
- [17] Tanabe T, Akamatsu D, Kobayashi T, Takamizawa A, Yanagimachi S, Ikegami T, Suzuyama T, Inaba H, Okubo S, Yasuda M, Hong F-L, Onae A, and Hosaka K 2015 Improved frequency measurement of the $^1\text{S}_0$ – $^3\text{P}_0$ clock transition in ^{87}Sr using a Cs fountain clock as a transfer oscillator *J. Phys. Soc. Jpn.* **84** 115002
- [18] Hachisu H, Petit G, Nakagawa F, Hanado Y, and Ido T 2017 SI-traceable measurement of an optical frequency at the low 10^{-16} level without a local primary standard *Opt. Express* **25** 8511-8523
- [19] McGrew W F, Zhang X, Leopardi H, Fasano R J, Nicolodi D, Beloy K, Yao J, Sherman J A, Schäffer S A, Savory J, Brown R C, Römisch S, Oates C W, Parker T E, Fortier T M, and Ludlow A D 2019 Towards the optical second: verifying optical clocks at the SI limit *Optica* **6** 448-454
- [20] Pizzocaro M, Bregolin F, Barbieri P, Rauf B, Levi F, and Calonico D 2019 Absolute frequency measurement of the $^1\text{S}_0$ – $^3\text{P}_0$ transition of ^{171}Yb with a link to International Atomic Time *Metrologia*
- [21] Hill I R, Hobson R, Bowden W, Bridge E M, Donnellan S, Curtis E A, and Gill P 2016 A low maintenance Sr optical lattice clock *J. Phys. Conf. Ser.* **723** 012019
- [22] Blatt S, Ludlow A D, Campbell G K, Thomsen J W, Zelevinsky T, Boyd M M, Ye J, Baillard X, Fouché M, Le Targat R, Brusch A, Lemonde P, Takamoto M, Hong F-L, Katori H, Flambaum V V 2008 New Limits on Coupling of Fundamental Constants to Gravity Using ^{87}Sr Optical Lattice Clocks *Phys. Rev. Lett.* **100** 140801
- [23] Safronova M S, Budker D, DeMille D, Jackson Kimball D F, Derevianko A, and Clark C W 2018 Search for new physics with atoms and molecules *Rev. Mod. Phys.* **90** 025008
- [24] Derevianko A and Pospelov M 2014 Hunting for topological dark matter with atomic clocks *Nat. Phys.* **10** 933-936
- [25] Wcisło P, Morzyński P, Bober M, Cygan A, Lisak D, Ciuryło R, and Zawada M 2016 Experimental constraint on dark matter detection with optical atomic clocks *Nat. Astron.* **1** 0009
- [26] Takamoto M, Ushijima I, Ohmae N, Yahagi T, Kokado K, Shinkai H, and Katori H 2020 Test of General Relativity by a Pair of Transportable Optical Lattice Clocks *Nat. Photon.*
- [27] Takano T, Takamoto M, Ushijima I, Ohmae N, Akatsuka T, Yamaguchi A, Kuroishi, Munekane H, Miyahara B, and Katori H 2016 Geopotential measurements with synchronously linked optical lattice clocks *Nat. Photon.* **10** 662-666
- [28] Grotti J *et. al.* 2018 Geodesy and metrology with a transportable optical clock *Nat. Phys.* **14** 437-441
- [29] Hachisu H, Nakagawa F, Hanado Y, and Ido T 2018 Months-long real-time generation of a time scale based on an optical clock *Sci. Rep.* **8** 4243
- [30] Milner W R, Robinson J M, Kennedy C J, Bothwell T, Kedar D, Matei D G, Legero T, Sterr U, Riehle F, Leopardi H, Fortier T M, Sherman J A, Levine J, Yao J, Ye J, and Melker E 2019 Demonstration of a Timescale Based on a Stable Optical Carrier *Phys. Rev. Lett.* **123** 173201
- [31] Yao J, Sherman J A, Fortier T, Leopardi H, Parker T, McGrew W, Zhang X, Nicolodi D, Fasano R, Schäffer S, Beloy K, Savory J, Romisch S, Oates C, Diddams S, Ludlow A, and Levine J 2019 Optical-Clock-Based Time Scale *Phys. Rev. Applied* **12** 044069
- [32] Inaba H, Daimon Y, Hong F-L, Onae A, Minoshima K, Schibli T R, Matsumoto H, Hirano M, Okuno T, Onishi M, and Nakazawa M 2006 Long-term measurement of optical frequencies using a simple, robust and low-noise fiber based frequency comb *Opt. Express* **14** 5223-5231
- [33] Hisai Y, Akamatsu D, Kobayashi T, Okubo S, Inaba H, Hosaka K, Yasuda M, and Hong F-L 2019 Development of 8-branch Er: fiber frequency comb for Sr and Yb optical lattice clocks *Opt. Express* **27** 6404-6414
- [34] Kobayashi T, Akamatsu D, Hosaka K, and Yasuda M 2019 A relocking scheme for optical phase locking using a digital circuit with an electrical delay line *Rev. Sci. Instrum.* **90** 103002

- [35] Kobayashi T, Akamatsu D, Hisai Y, Tanabe T, Inaba H, Suzuyama T, Hong F-L, Hosaka K, and Yasuda M 2018 Uncertainty Evaluation of an ^{171}Yb Optical Lattice Clock at NMIJ *IEEE Trans. Ultrason. Ferroelectr. Freq. Control* **65** 2449-2458
- [36] Katori H, Takamoto M, Pal'chikov V G, and Ovsiannikov V D 2003 Ultrastable optical clock with neutral atoms in an engineered light shift trap *Phys. Rev. Lett.* **91** 173005
- [37] Kobayashi T, Akamatsu D, Hosaka K, Inaba H, Okubo S, Tanabe T, Yasuda M, Onae A, and Hong F-L 2016 Absolute frequency measurements and hyperfine structures of the molecular iodine transitions at 578 nm *J. Opt. Soc. Am. B* **33** 725-734
- [38] Saxberg B, Plotkin-Swing B, and Gupta S Active stabilization of a diode laser injection lock 2016 *Rev. Sci. Instrum.* **87** 063109
- [39] Kobayashi T, Akamatsu D, Nishida Y, Tatabe T, Yasuda M, Hong F-L, and Hosaka K 2016 Second harmonic generation at 399 nm resonant on the $^1S_0 - ^1P_0$ transition of ytterbium using a periodically poled LiNbO_3 waveguide *Opt. Express* **24** 12142-12150
- [40] Iwakuni K, Inaba H, Nakajima Y, Kobayashi T, Hosaka K, Onae A, and Hong F-L 2012 Narrow linewidth comb realized with a mode-locked fiber laser using an intra-cavity waveguide electro-optic modulator for high-speed control *Opt. Express* **20** 13769-13776
- [41] Inaba H, Hosaka K, Yasuda M, Nakajima Y, Iwakuni K, Akamatsu D, Okubo S, Kohno T, Onae A, and Hong F-L 2013 Spectroscopy of ^{171}Yb in an optical lattice based on laser linewidth transfer using a narrow linewidth frequency comb *Opt. Express* **21** 7891-7896
- [42] Hisai Y, Ikea K, Sakagami H, Horikiri T, Kobayashi T, Yoshii K, and Hong F-L 2018 Evaluation of laser frequency offset locking using an electrical delay line *Appl. Opt.* **57** 5628-5634
- [43] Akamatsu D, Inaba H, Hosaka K, Yasuda M, Onae A, Suzuyama T, Amemiya M, and Hong F-L 2013 Spectroscopy and frequency measurement of the ^{87}Sr clock transition by laser linewidth transfer using an optical frequency comb *Appl. Phys. Express* **7** 012401
- [44] Katori H, Ovsiannikov V D, Marmo S I, and Palchikov V G 2015 Strategies for reducing the light shift in atomic clocks *Phys. Rev. A* **91** 052503
- [45] Nemitz N, Ohkubo T, Takamoto M, Ushijima I, Das M, Ohmae N, and Katori H 2016 Frequency ratio of Yb and Sr clocks with 5×10^{-17} uncertainty at 150 seconds averaging time *Nat. Photon.* **10** 258-261
- [46] Nemitz N, Jørgensen A A, Yanagimoto R, Bregolin F, and Katori H 2019 Modeling light shifts in optical lattice clocks *Phys. Rev. A* **99** 033424
- [47] Brown R C, Phillips N B, Beloy K, McGrew W F, Schioppo M, Fasano R J, Milani G, Zhang X, Hinkley N, Leopardi H, Yoon T H, Nicolodi D, Fortier T M, and Ludlow A D 2017 Hyperpolarizability and Operational Magic Wavelength in an Optical Lattice Clock *Phys. Rev. Lett.* **119** 253001
- [48] Blatt S, Thomsen J W, Campbell G K, Ludlow A D, Swallows M D, Martin M J, Boyd M M, and Ye J 2009 Rabi spectroscopy and excitation inhomogeneity in a one-dimensional optical lattice clock *Phys. Rev. A* **80** 052703
- [49] Kim H, Heo M-S, Lee W-K, Park C Y, Hong H-G, Hwang S-W, and Yu D-H 2017 Improved absolute frequency measurement of the ^{171}Yb optical lattice clock at KRISS relative to the SI second *Jpn. J. Appl. Phys.* **56** 050302
- [50] Middelmann T, Lisdat C, Falke S, Vellore Winfred J S R, Riehle F, and Sterr U 2011 Tackling the blackbody shift in a strontium optical lattice clock *IEEE Trans. Instrum. Meas.* **60** 2550
- [51] Sherman J A, Lemke N D, Hinkley N, Pizzocaro M, Fox R W, Ludlow A D, and Oates C W 2012 High-Accuracy Measurement of Atomic Polarizability in an Optical Lattice Clock *Phys. Rev. Lett.* **108** 153002
- [52] Beloy K, Hinkley N, Phillips N B, Sherman J A, Shioppo M, Lehman J, Feldman A, Hanssen L M, Oates C W, Ludlow A D 2014 Atomic Clock with 1×10^{-18} Room-Temperature Blackbody Stark Uncertainty *Phys. Rev. Lett.* **113** 260801
- [53] Lemke N D, von Stecher J, Sherman J A, Rey A M, Oates C W, and Ludlow A D 2011 p -Wave Cold Collisions in an Optical Lattice Clock *Phys. Rev. Lett.* **107** 103902

- [54] Ludlow A D, Lemke N D, Sherman J A, Oates C W, Quémener G, von Stecher J, and Rey A M 2011 Cold-collision-shift cancellation and inelastic scattering in a Yb optical lattice clock *Phys. Rev. A* **84** 052724
- [55] Lee S, Park C Y, Lee W-K, and Yu D-H 2016 Cancellation of collisional frequency shifts in optical lattice clocks with Rabi spectroscopy *New J. Phys.* **18** 033030
- [56] Nakajima Y, Inaba H, Hosaka K, Minoshima K, Onae A, Yasuda M, Kohno T, Kawato S, Kobayashi T, Katsuyama T, and Hong F-L 2010 A multi-branch, fiber-based frequency comb with millihertz-level relative linewidths using an intra-cavity electro-optic modulator *Opt. Express* **18** 1667-1676
- [57] <https://www.bipm.org/en/bipm/tai/>.
- [58] Yu D-H, Weisse M, and Parker T E 2007 Uncertainty of a frequency comparison with distributed dead time and measurement interval offset *Metrologia* **44** 91-96
- [59] Bauch A 2005 The PTB primary clocks CS1 and CS2 *Metrologia* **42** S43-S54
- [60] Guéna J, Abgrall M, Rovera D, Laurent P, Chupin B, Lours M, Santarelli G, Rosenbusch P, Tobar M E, Li R, Gibble K, Clairon A, and Bize S 2012 Progress in atomic fountains at LNE-SYRTE *IEEE Trans. Ultrason. Ferroelectr. Freq. Control* **59** 391-409
- [61] Weyers S, Gerginov V, Kazda M, Rahm J, Lipphardt B, Dobrev G, and Gibble K 2018 Advances in the accuracy, stability, and reliability of the PTB primary fountain clocks *Metrologia* **55** 789-805
- [62] Blinov I Y, Boiko A I, Domnin Y S, Kostromin V P, Kupalova O V, and Kupalov D S 2017 Budget of Uncertainties in the Cesium Frequency Frame of Fountain Type *Measurement Techniques* **60** 30-36
- [63] Fang F, Li M, Lin P, Chen W, Liu N, Lin Y, Wang P, Liu K, Suo R, and Li T 2015 NIM5 Cs fountain clock and its evaluation *Metrologia* **52** 454-468
- [64] Guéna J, Abgrall M, Clairon A, and Bize S 2014 Contributing to TAI with a secondary representation of the SI second *Metrologia* **51** 108-120
- [65] Hachisu H, Petit G, and Ido T 2016 Absolute frequency measurement with uncertainty below 1×10^{-15} using International Atomic Time *Appl. Phys. B* **123** 34
- [66] Kohno T, Yasuda M, Hosaka K, Inaba H, Nakajima Y, and Hong F-L 2009 One-Dimensional Optical Lattice Clock with a Fermionic ^{171}Yb Isotope *Appl. Phys. Express* **2** 072501
- [67] Yasuda M, Inaba H, Kohno T, Tanabe T, Nakajima Y, Hosaka K, Akamatsu D, Onae A, Suzuyama T, Amemiya M, and Hong F-L 2012 Improved Absolute Frequency Measurement of the ^{171}Yb Optical Lattice Clock towards a Candidate for the Redefinition of the Second *Appl. Phys. Express* **5** 102401
- [68] Park C Y, Yu D-J, Lee W-K, Park S E, Kim E B, Lee S K, Cho J W, Yoon T H, Mun J, Park S J, Kwon T Y, and Lee S-B 2013 Absolute frequency measurement of $^1\text{S}_0(F=1/2)-^3\text{P}_0(F=1/2)$ transition of ^{171}Yb atoms in a one-dimensional optical lattice at KRISS *Metrologia* **50** 119-128
- [69] Akamatsu D, Yasuda M, Inaba H, Hosaka K, Tanabe T, Onae A, and Hong F-L 2014 Frequency ratio measurement of ^{171}Yb and ^{87}Sr optical lattice clocks *Opt. Express* **22** 7898-7905
- [70] Takamoto M, Ushijima I, Das M, Nemitz N, Ohkubo T, Yamanaka K, Ohmae N, Takano T, Akatsuka T, Yamaguchi A, and Katori H 2015 Frequency ratios of Sr, Yb, and Hg based optical lattice clocks and their applications *C. R. Phys.* **16** 489-498
- [71] Fujieda M, Yang S-H, Gotoh T, Hwang S-W, Hachisu H, Kim H, Lee Y K, Tabuchi R, Ido T, Lee W-K, Heo M-S, Park C Y, Yu D-H, and Petit G 2018 Advanced satellite-based frequency transfer at the 10^{-16} level *IEEE Trans. Ultrason. Ferroelectr. Freq. Control* **65** 973-978
- [72] Akamatsu D, Kobayashi T, Hisai Y, Tanabe T, Hosaka K, Yasuda M, and Hong F-L 2018 Dual-mode operation of an optical lattice clock using strontium and ytterbium atoms *IEEE Trans. Ultrason. Ferroelectr. Freq. Control* **65** 1069-1075
- [73] Peil S, Crane S, Hanssen J L, Swanson T B, and Ekstrom C R 2013 Tests of local position invariance using continuously running atomic clocks *Phys. Rev. A* **87** 010102(R)
- [74] Takamizawa A, Yanagimachi S, Tanabe T, Hagimoto K, Hirano I, Watabe K, Ikegami T, and Hartnett J G 2015 Preliminary Evaluation of the Cesium Fountain Primary Frequency Standard NMIJ-F2 *IEEE Trans. Instrum. Meas.* **64** 2504-2512

- [75] Wcisło P *et al.* 2018 New bounds on dark matter coupling from a global network of optical atomic clocks *Sci. Adv.* **4**, eaau4869
- [76] Roberts B M *et al.* 2019 Search for transient variations of the fine structure constant and dark matter using fiber-linked optical atomic clocks arXiv:1907.02661